THE TESLA DETECTOR CONCEPT*

M.A. Thomson,
Cavendish Laboratory, University of Cambridge, Cambridge, UK

Abstract

The high precision physics goals of a future $\mathrm{e^+e^-}$ linear collider place strict requirements on the design of the detector. This paper gives an overview of the TESLA detector concept concentrating on the physics motivation for the design choice and the detector performance.

INTRODUCTION

Within the particle physics community there is increasing consensus that the world's next large accelerator project will be an $\mathrm{e^+e^-}$ linear collider (LC) operating in the energy range 500 GeV−1 TeV. The TESLA (TeV Energy Superconducting Linear Accelerator) project [1] offers one technological route to realising such a LC. The luminosities provided by TESLA would be approximately three orders of magnitude greater than those achieved at LEP. This, coupled with the clean environment of $\mathrm{e^+e^-}$ collisions, would make TESLA the ideal place for precision studies of physics beyond the Standard Model (SM). The physics potential of a LC, such as understanding the nature of any Higgs-like particle, places stringent requirements on all aspects of the detector design.

*This article summarises both detector R&D work and the studies of the impact of the detector performance on the physics potential of the TESLA linear collider. Much of the work was performed in the extended ECFA/DESY study by: K. Ackermann, L. Andricek, H.M. Araujo, S. Ask, J.E. Augustin, M. Battaglia, H. Bauke, M. Baulillier, T. Behnke, A.C. Benvenuti, M. Berggren, J.-D. Berst, F. Bieser, G. Blair, W. de Boer, A. Bondar, I. Bozovic, J.C. Brient, I. Britvich, K. Buesser, A. Buzulutskov, T. Camporesi, B. Canton, R.C. Carnegie, C. Carimalo, P. Checchia, R. Cizeron, G. Claus, P. Cloarec, P. Colas, C. Colledani, C. Damerell, A. Delbart, G. Deptuch, F. Le Diberder, M.S. Dixit, V. Djordjadze, M. Doucet, J. Dubeau, W. Dulinski, W. Da Silva, V. Eckardt, W. Edwards, M. Elsing, C. Fanin, A. Feniouk, P. Fischer, B. Gastineau, P. Gay, G. Genolini, N. Ghodbane, Y. Giomataris, U. Goerlach, Y. Gornushkin, H. van der Graaf, N. de Groot, M. Gruwe, P. Hassler, M. Hamann, K. Harder, J. Hauschildt, R. Hawkings, V. Hedberg, Y. Hu, D. Husson, D. Imbault, A. Imhof, D.J. Jackson, J. Jeanjean, J. Kaminski, A. Kaoukher, S. Kappler, F. Kapusta, A. Karar, D. Karlen, M. Killenberg, F. Kircher, V. Klioukhine, M. Kock, V. Korbel, T. Kuhl, J. Kuhlmann, H. Lebbolo, B. Ledermann, V. Lepeltier, V. Lishin, S. Lotze, G. Lutz, T. Lux, S. Magill, M. Margoni, C. Martens, J.-P. Martin, M. Mazzucato, H. Mes, N. Meyners, D.J. Miller, J. Mnich, K. Moenig, S. Monteil, P. Mora de Freitas, V. Morgunov, T. Müller, D. Nygren, G. Orazi, V. Obraztsov, D. Orlando, Y. Pabot, M. Paganoni, J. Peyré, M. Pohl, V. Poliakov, V. Popov, J. Pouthas, P. Rebourgeard, D. Reid, R. Richter J.-L. Riester M. Ronan, F. Rossel, S. Roth, K. Sachs, V. Saveliev, A. Savoy-Navarro, H.J. Schreiber, H. Schröder, R. Schulte, M. Schumacher R. Settles, L. Shekhtman, M. Siemens, F. Simonetto K. Sinram, B. Sobloher, A. Stahl, K. Stefanov, W. Struczinski, S. Shuvalov, Ch. de la Taille, V.I. Telnov, F. Terranova, J. Timmermans, M. Tonutti, M. Trimpl, R. Turchetta, J. Ulrici, A. Vasilev, H. Videau, D. Vincent, E. Vlasov, N. Wermes, D. Wicke, M. Wing, M. Winter H. Wieman, S.M. Xella-Hansen, R. Zimmermann

THE PHYSICS ENVIRONMENT

It is foreseen that the TESLA LC would operate at centre-of-mass energies of $90-800\,\mathrm{GeV}$. In the TESLA design, the colliding beams arrive in five bunch trains per second with each train consisting of 2820 bunches separated by 337 ns. The nominal luminosity (at 500 GeV) is $3.4\times10^{34}\,\mathrm{cm^{-2}\,s^{-1}}$ which is more than 1000 times that achieved at LEP 2. The corresponding event rates are indicated in Table 1. In addition to the listed processes there is a significant background from the multi-peripheral "two photon" process, $\mathrm{e^+e^-} \rightarrow \mathrm{e^+e^-} + \mathrm{hadrons}$, which corresponds to approximately 0.02 events with visible tracks per bunch crossing (BX) at 500 GeV. The relatively long time between successive BXs (337 ns) should allow association of tracks with BX. In addition to the two photon background, there are also significant beam related backgrounds corresponding to approximately 600 hits per BX in the Vertex detector. These background levels, although high compared to those experienced at LEP, are much lower than those anticipated at the LHC. Consequently the detector design is dictated by the physics goals and not by issues of radiation hardness.

Table 1: Event rates at a 500 GeV $\mathrm{e^+e^-}$ collider assuming the TESLA design luminosity of $3.4\times10^{34}\,\mathrm{cm^{-2}\,s^{-1}}$. The event rate from $\mathrm{e^+e^-} \rightarrow \mathrm{q\overline{q}}$ refers to the rate summed over all quarks other than the top quark.

Process	**Event Rate**
$\mathrm{e^+e^-} \rightarrow \mathrm{e^+e^-}$ ($\theta > 20$ mrad)	350 $\mathrm{s^{-1}}$
$\mathrm{e^+e^-} \rightarrow \mathrm{q\overline{q}}$	1600 $\mathrm{h^{-1}}$
$\mathrm{e^+e^-} \rightarrow \mathrm{W^+W^-}$	930 $\mathrm{h^{-1}}$
$\mathrm{e^+e^-} \rightarrow \mathrm{t\overline{t}}$	70 $\mathrm{h^{-1}}$
$\mathrm{e^+e^-} \rightarrow \mathrm{ZH}$ (M_H=120 GeV)	7 $\mathrm{h^{-1}}$

PHYSICS AT A LINEAR COLLIDER

The physics case for a future LC is well documented in the TESLA Technical Design Report [1] (TDR). The main goals of the physics programme are summarised below:

- *Higgs Physics:* If the Higgs boson exists, it is likely that it will be discovered at the LHC or Tevatron. At a LC the emphasis will be on establishing the nature of the Higgs through precise measurements of its properties, such as mass, fermionic branching fractions and the Higgs boson trilinear coupling.
- *Supersymmetry:* Supersymmetry (SUSY) is a widely touted candidate for physics beyond the SM. How-

ever, SUSY encompasses a wide range of theoretical scenarios, both in terms of the mechanism by which SUSY is broken and the large number of free parameters within SUSY models. The wealth of precise measurements possible at the LC would provide a powerful probe of the underlying structure of the SUSY theory.

- *Strong Electroweak Symmetry Breaking:* If the Higgs boson is not discovered at the LHC or Tevatron, an alternative mechanism for electroweak symmetry breaking is required. The golden physics process in the absence of the Higgs boson is that of longitudinal W-boson scattering, $\mathrm{W}_\mathrm{L}^+\mathrm{W}_\mathrm{L}^- \rightarrow \mathrm{W}_\mathrm{L}^+\mathrm{W}_\mathrm{L}^-$ which, without contributions from the s-channel Higgs exchange, grows and violates quantum mechanical unitarity. To avoid unitarity violation it is required that the interactions between the vector-bosons become strong at energies of order 1 TeV. This would be manifested in anomalous triple or quartic gauge boson couplings. Observation of the $\mathrm{W}^+\mathrm{W}^-$ and ZZ scattering processes will be possible using the final states $\nu_e\overline{\nu}_e\mathrm{W}^+\mathrm{W}^-$ and $\nu_e\overline{\nu}_e\mathrm{ZZ}$. Anomalous gauge boson couplings can be studied using similar techniques to those used at LEP, such as the reconstruction of angular distributions and correlations.

- *Top-quark Physics:* An $\mathrm{e}^+\mathrm{e}^-$ LC provides a clean environment in which to study the properties of the top quark. In particular, the mass of the top quark is a key input in fits to high precision electroweak data. At the LC the top quark mass can be determined with a precision of $\sim$ 200 MeV compared to $1-2$ GeV at LHC.

DETECTOR REQUIREMENTS

Before considering explicitly the requirements for a detector at a future LC it is worth considering the impact of the performance of the LEP detectors on the physics sensitivity. The main goal at LEP was to perform precision measurements of the properties of the W and Z gauge bosons. Physics sensitivity did not usually depend strongly on the detector performance. A good example is the measurement of the W-boson mass where the four LEP collaborations obtain similar statistical uncertainties [2] with significantly different jet energy resolutions. This is a direct consequence of the kinematic fit where the total energy of the final state fermions is constrained to be equal to the energy of the $\mathrm{e}^+\mathrm{e}^-$ collisions; as a result the mass resolution is significantly better than achieved using the raw measured jet energies, as indicated in Fig. 1 [3]. At a LC, kinematic fitting will be far less useful due to Beamstrahlung and increased initial state radiation (ISR). In addition, many of the potentially interesting final states at a future LC involve two or more unobserved particles, for example, $\mathrm{e}^+\mathrm{e}^- \rightarrow \nu_e\overline{\nu}_e\mathrm{W}^+\mathrm{W}^-$ and many SUSY processes, and kinematic constraints will be of limited use. As a result, the physics performance at a LC depends critically on being able to reconstruct the gauge bosons directly from jets and leptons. This places strict performance requirements on the detector.

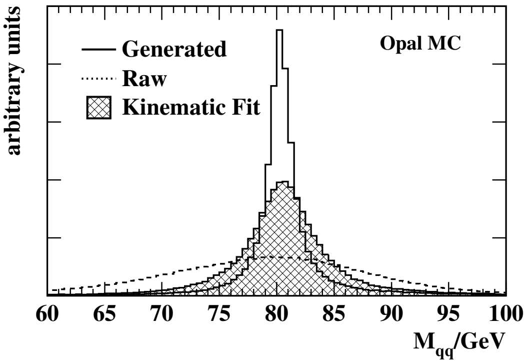

Figure 1: A comparison of the reconstructed invariant mass distribution from the $\mathrm{q}\overline{\mathrm{q}}$ system in $\mathrm{W}^+\mathrm{W}^-\rightarrow\mathrm{q}\overline{\mathrm{q}}\ell\overline{\nu}_\ell$ events at LEP using the measured quantities (Raw) and the result of the kinematic fit [3]. Also shown is the underlying generated distribution.

Detector Requirements at TESLA

The main requirements for a TESLA detector are summarised below:

- *Momentum resolution:* $\sigma_{1/p} \sim 5\times10^{-5}\,\mathrm{GeV}^{-1}$ (a factor of ten better than that achieved at LEP). Good momentum resolution is important for the reconstruction of the leptonic decays of Z bosons. This is particularly relevant for $\mathrm{e}^+\mathrm{e}^- \rightarrow \mathrm{ZH}$ events where the Higgs boson properties, including its mass, are best studied by considering the system recoiling against the Z, with the golden channel being $\mathrm{Z}\rightarrow\mu^+\mu^-$.

- *Impact parameter resolution:* Efficient b and c quark tagging which implies good impact parameter (d_0) resolution:

$$\sigma_{d_0}^2 < (5.0\,\mu\mathrm{m})^2 + \left(\frac{5.0\,\mu\mathrm{m}}{p(\mathrm{GeV})\sin^{\frac{3}{2}}\theta}\right)^2.$$

  This is a factor of three better resolution than obtained at SLD.

- *Jet energy resolution:* $\sigma_E/E \sim 0.3/\sqrt{E(\mathrm{GeV})}$ in order to be able to directly reconstruct and identify gauge bosons from their hadronic decays to jets, *i.e.* $\mathrm{W}\rightarrow\mathrm{q}\overline{\mathrm{q}}$ and $\mathrm{Z}\rightarrow\mathrm{q}\overline{\mathrm{q}}$. This is a factor of two better than the best achieved at LEP.

- *Hermiticity:* Hermetic down to 5 mrad for searches for missing energy signals from new physics.

- *High Granularity:* Events at the LC will have high track densities due to the boosted final states and the fact that many of the interesting physics processes result in final states with six or more jets. A LC detector is required to have high granularity and good two track resolution.

THE TESLA DETECTOR CONCEPT

The baseline TESLA detector concept is discussed in detail in the TESLA TDR [1]. The general detector layout consists of a cylindrical barrel region and two endcaps and is shown in Fig. 2. Tracking of charged particles is performed using a high precision Silicon-based microvertex detector (VTX) surrounded by a large gaseous time projection chamber (TPC) which provides a large number of space points along a track and enables momentum determination. The tracking is supplemented by additional Silicon forward tracking detectors (FTD) perpendicular to the beam axis. The high granularity electromagnetic calorimeter (ECAL) consists of alternate layers of Silicon and Tungsten. A high granularity hadronic calorimeter (HCAL) is located outside the ECAL, but still inside the magnet coil. The superconducting magnet, which is based on the CMS magnet [4], provides a highly homogeneous 4 T solenoidal field. Muon chambers are located within the magnet return yoke. There is no hardware trigger, with deadtime-free continuous readout over a complete 1 ms bunch train. Zero suppression, hit recognition and digitisation is performed in the front-end electronics.

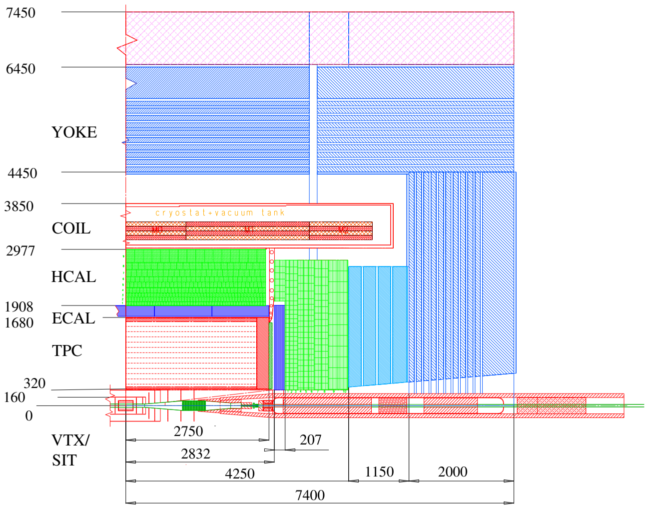

Figure 2: A quadrant of the TDR concept of a detector for TESLA [1] (dimensions in mm).

The main features of the detector components are described below, concentrating on the tracking detectors, in particular the vertex detector and central tracker, and the calorimetry.

OVERVIEW OF THE TRACKING SYSTEM

The primary requirements of the tracking system for a detector at TESLA are: excellent momentum resolution, $\sigma_{1/p} \sim 5 \times 10^{-5}\,\mathrm{GeV}^{-1}$; excellent heavy flavour tagging capability and efficient track reconstruction down to small angles. A subsidiary, but nevertheless important, requirement is to minimise the amount of material in the central tracker in order to minimise multiple scattering, to reduce the occupancy from converting background photons, and to avoid compromising the performance of the calorimeters. The components of the tracking system are:

- a multilayer micro-vertex detector (VTX) from radii of $1.5 - 6.0$ cm consisting of five concentric barrels of Silicon pixel detectors;
- a large volume Time Projection Chamber (TPC) between radii $32 - 170$ cm to provide precise momentum measurements;
- additional Silicon tracking between the vertex detector and the TPC consisting of 2 cylinders of Silicon in the barrel region (SIT) and discs in the forward region (FTD);
- a precise forward straw chamber or Silicon tracker behind the TPC endplate (FCH/Si-FCH).

The layout of the tracking system is shown in Fig. 3. One advantage of the proposed system is that tracks can be reconstructed independently in the TPC and in the combined seven layers of the VTX and SIT detectors, thus aiding both alignment and calibration. The physics motivation and the design of the main components of the tracking system are described below.

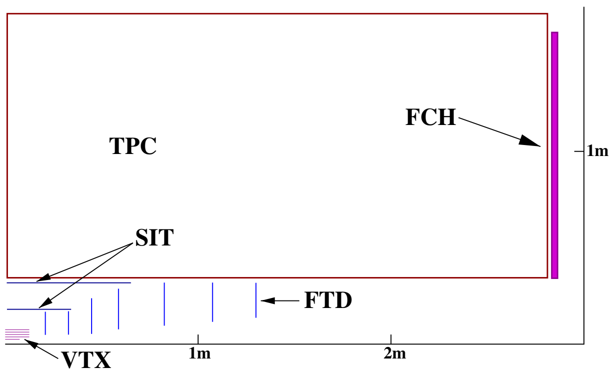

Figure 3: The components of the tracking system [1].

VERTEX DETECTOR

Precise measurements of the properties of as yet undiscovered new particles form the cornerstone of the LC physics programme. It is assumed that if the Higgs boson and/or SUSY exist, they are likely to have been discovered at the LHC or Tevatron before the linear collider is operational. At a LC the emphasis will be on establishing the nature of these new particles by making precise measurements of their properties. Heavy-flavour tagging will be of prime importance in many of these studies as many signatures of new physics result in final states containing b-quarks, for example, $\mathrm{e^+e^-} \to \mathrm{ZHH}$ and $\mathrm{e^+e^-} \to \mathrm{H^0A^0} \to \mathrm{b\overline{b}b\overline{b}}$. One particularly important question is whether the Higgs boson, if it is observed, has production and decay properties consistent with being the SM Higgs. In the SM the Higgs boson coupling to fermions, g_{Hff}, is proportional to the fermion mass. If the Higgs boson is light ($M_{\mathrm{H}} < 150\,\mathrm{GeV}$), which is consistent with the current electroweak data [2], one important test of the Higgs sector will be the measurement of its fermionic branching fractions, shown in Fig. 4. Here the ability to be able to tag efficiently charm quarks is important for separating $\mathrm{H} \to \mathrm{c\overline{c}}$ and $\mathrm{H} \to \mathrm{b\overline{b}}$. Efficient heavy flavour tagging will also play a major rôle in the event identification of many final states involving quarks.

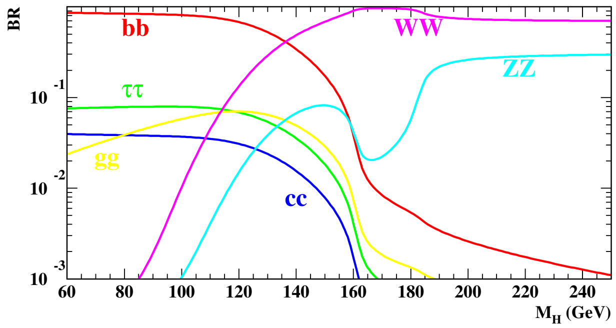

Figure 4: The decay branching fractions of the SM Higgs boson as a function of Higgs boson mass, M_{H}.

Design Issues

Heavy flavour tagging requires a precise measurement of the impact parameter d_0, the transverse $(r\phi)$, distance of a charged particle track from the primary vertex. In general, the impact parameter resolution can be expressed as the quadrature sum of two terms:

$$\sigma_{d_0}^2 = a^2 + \left(\frac{b}{p(\mathrm{GeV})\sin^{\frac{3}{2}}\theta}\right)^2.$$

The first term, a, depends on the single point resolution and the second term is the degradation in resolution arising from multiple scattering in the vertex detector which depends on both polar angle θ and momentum p. The TESLA detector goal is for both a and b to be smaller than $\sim 5\,\mu$m. This would represent a significant improvement over previous vertex detectors, *e.g.* this is approximately a factor three better than that achieved at SLD.

In light of the success of the SLD vertex detector it is generally accepted that a vertex detector at the next linear collider will consist of approximately one billion Silicon pixels arranged in concentric cylindrical layers, as shown schematically in Fig. 5.

Given the rapid evolution of semi-conductor devices, it is too early to decide on a specific detector technology, however there are a number of widely accepted design principles:

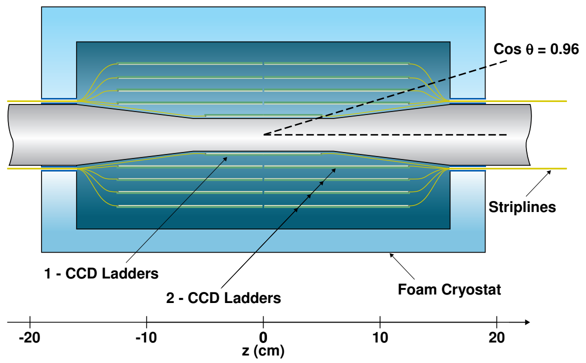

Figure 5: General layout of a CCD-based vertex detector [1].

- the inner layer should be as close to the interaction region as possible. This is particularly important for charm tagging. In the TESLA TDR design [1] the inner radius is 15 mm. Ultimately the minimum inner radius is determined by the size of the beam pipe, which depends on the accelerator design.

- at TESLA beam related backgrounds, even at a radius of 12.5 mm, are not a significant problem as most $\mathrm{e^+e^-}$ pairs from beam-beam interactions are confined to the beam pipe by the 4 T magnetic field.

- the detector should consist of five layers to allow full track reconstruction independent of the central tracking chamber.

- space points should be measured with a precision of $< 5\,\mu\mathrm{m}$ which is obtainable with CCD pixel sizes of $\sim 20 \times 20\,\mu\mathrm{m}^2$ by charge centroid fitting. In addition, to giving to good space point resolution, a small pixel size is important to separate hits from multiple tracks in dense event environments, *e.g.* the cores of high multiplicity jets.

- the thickness of the layers should be reduced from $0.004\,X_0$ (SLD) to less than $0.001\,X_0$. This not only improves the d_0 resolution by reducing multiple scattering, but also suppresses γ conversions allowing clean electron identification in heavy flavour decays.

Although the general concept and performance goals are well defined the technological route is uncertain and forms an active area of research and development. The main options currently being considered are: CCD pixel devices [5]; CMOS monolithic active pixel sensors (MAPS) [6]; hybrid active pixel sensors (HAPS) [7] and depleted Field Effect Transistors (DEPFET) [8].

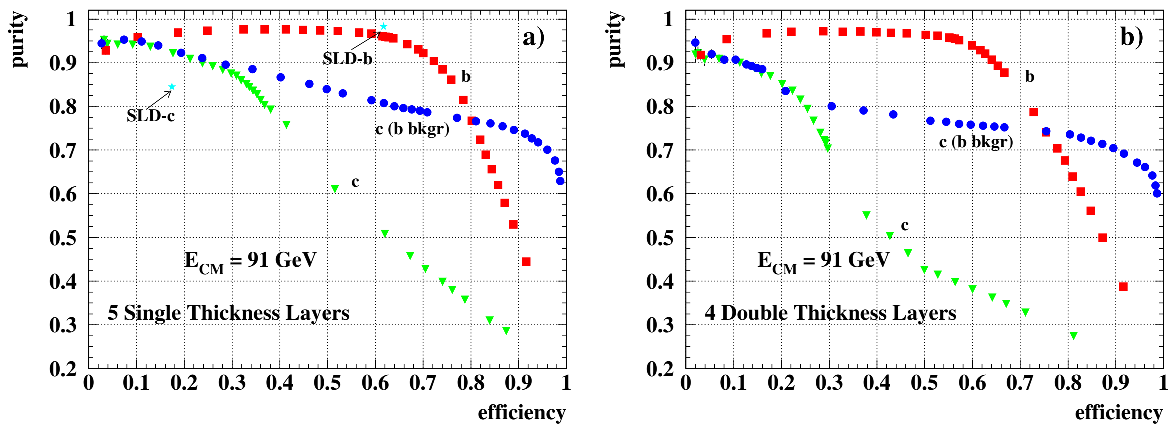

Figure 6: Efficiency and purity for tagging a heavy flavour jet in Z decays [10]. Figure a) shows the performance of a slightly modified version of the TDR VTX detector. Figure b) shows the degradation in performance if the inner layer is removed and the layer thickness doubled. The c(b bkgr) points represent the charm tagging efficiency when only bottom jets constitute the background. For comparison the best results from SLD are also indicated.

Performance

The baseline VTX detector of the TESLA TDR consists of 5 concentric cylinders of $20 \times 20\,\mu\mathrm{m}^2$ CCD pixels located at radii of 15 mm, 26 mm, 38 mm, 48 mm and 60 mm. Each layer corresponds to a thickness of 0.06 % of a radiation length. The expected performance of such a device has been evaluating using the sophisticated tracking and heavy flavour tagging algorithms [9, 10] developed at LEP and SLD. For the TDR baseline design the impact parameter resolution is

$$\sigma_{d_0}^2 = (4.2\,\mu\mathrm{m})^2 + \left(\frac{4.0\,\mu\mathrm{m}}{p(\mathrm{GeV})\sin^{\frac{3}{2}}\theta}\right)^2.$$

For comparison the values obtained for the SLD detector were $a = 9\,\mu\mathrm{m}$ and $b = 38\,\mu\mathrm{m}$. The flavour tagging used in the TESLA studies is based primarily on the ZVTOP [11] topological vertexing method pioneered at SLD. This algorithm parametrises tracks as Gaussian probability tubes in three dimensional space and identifies vertices as regions of high tube overlap. In addition to ZVTOP, a 1-prong charm tag and an impact parameter joint probability tag [12] are combined in a neural net approach similar to that used by OPAL [13]. Recent studies [10] using the GEANT3 [14] based BRAHMS [15] simulation and these sophisticated (*i.e.* realistic) tagging algorithms compared the performance of different VTX detector configurations. Fig. 6a) shows the simulated heavy flavour tagging performance for a slightly modified version of the TDR VTX detector for a single jet in $\mathrm{Z} \to \mathrm{q\overline{q}}$ events. Although the b-tagging performance is similar to that obtained at SLD, there is a significant improvement of the charm tag; in the high purity region the charm tagging efficiency is approximately a factor two better than that obtained at SLD. Good charm tagging is particularly important for the Higgs to fermion pair branching ratio measurement. Fig. 6b shows the charm tagging efficiency versus purity curves obtained for a four layer VTX detector with the inner layer at 2.7 mm. In this case the layers have double the nominal thickness, *i.e.* $0.11\,\%\,X_0$. The charm tagging performance is significantly degraded. Other detector configurations have been studied [10] and the most important factor influencing the VTX detector performance is having the inner layer as close to the interaction region as possible.

THE CENTRAL TRACKER

The main purpose of the large volume central tracker is to provide precise momentum measurements. The performance requirements are set by the ability to reconstruct precisely Z bosons from their leptonic decays. This is particularly important for measurements of the properties of the Higgs boson. Current SM fits to electroweak data from LEP, the Tevatron and SLD suggest a relatively light Higgs boson mass, $M_{\mathrm{H}} < 219\,\mathrm{GeV}$ (95 % confidence level) [2]. In this mass range the cross-section for the SM Higgs-strahlung process, $\mathrm{e^+e^-} \to \mathrm{Z^*} \to \mathrm{ZH}$, shown in Fig. 7, is relatively large (a few tens of fb at $\sqrt{s} = 500\,\mathrm{GeV}$).

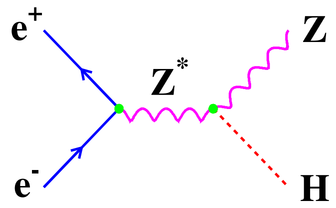

Figure 7: The SM Higgs-strahlung process. Note at a future linear collider the SM Higgs boson is also produced in the WW fusion process and to a lesser extent in the ZZ fusion process.

The Higgs boson typically decays into final states in-

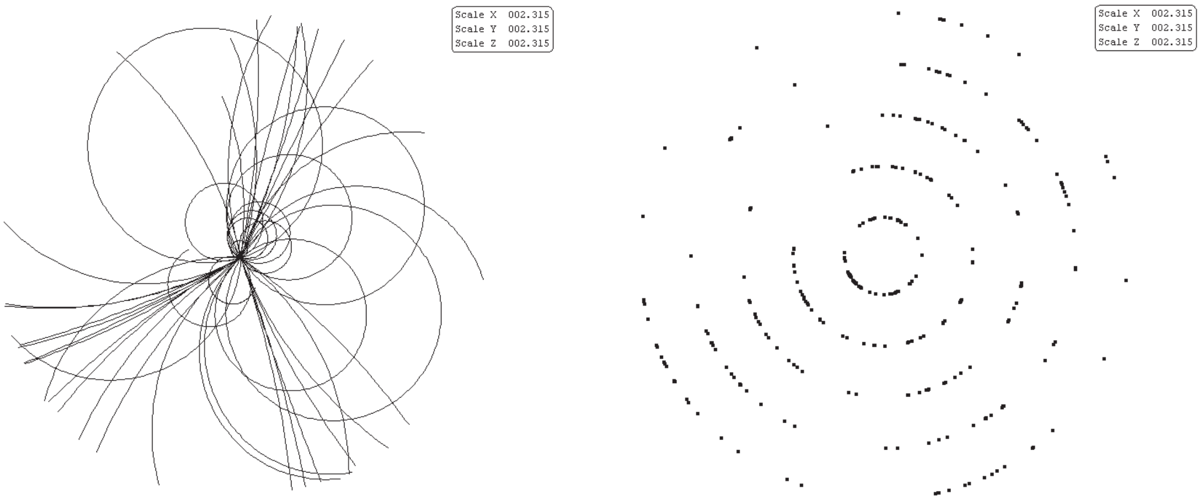

Figure 8: a) A typical linear collider event as seen in a TPC with sampling in more than 100 radial layers. b) The same event as seen in a 5 layer Silicon tracker.

volving jets (*e.g.* $\mathrm{H} \rightarrow \mathrm{b}\overline{\mathrm{b}}$ or for higher Higgs masses $\mathrm{H} \rightarrow \mathrm{W}^+\mathrm{W}^-$). As jet energies are relatively poorly measured the most precise measurements of the Higgs boson properties can be obtained from well measured Z decays. Consequently, the "golden" channel is the Higgs-strahlung process with $\mathrm{Z} \rightarrow \mu^+\mu^-$. Such events can be precisely reconstructed, independent of the Higgs decay mode, from the $\mu^+\mu^-$ system. For example, the mass of the Higgs boson can be determined from the mass recoiling against the $\mu^+\mu^-$ system. Two factors determine the precision of this measurement: the Z width, Γ_{Z}, and the event-by-event measurement error on the recoil mass which is of order the momentum resolution, σ_{p}. For the momentum resolution term to be significantly smaller than that from Γ_{Z} imposes the requirement on the momentum resolution of the entire tracking system (including the precisely measured hits in the VTX and SIT detectors) of $\sigma_{1/\mathrm{p}} \sim 5 \times 10^{-5}\,\mathrm{GeV}^{-1}$. This is an order of magnitude better than achieved at LEP. To achieve this goal, the momentum resolution from the central tracking chamber alone must be $\sigma_{1/\mathrm{p}} \sim 2 \times 10^{-4}\,\mathrm{GeV}^{-1}$.

Choice of Central Tracker Technology

A number of options for the large volume central tracker have been considered. These fall into two main categories: i) gaseous detectors which provide a large number of relatively coarse spatial measurements along a charged particle track and ii) Silicon detectors which provide a few very precise measurements. The TESLA baseline choice is a Time Projection Chamber (TPC) such as those successfully operated by the ALEPH [16] and DELPHI [17] collaborations at LEP. A TPC has a number of significant advantages:

- it provides a large number of three-dimensional space points which enables good pattern recognition in a dense track environment. This point is illustrated by Fig. 8, where the TPC hit pattern is compared with that which would be observed using a 5 layer Silicon central tracker.
- it provides adequate two hit resolution enabling separation of nearby charged particle tracks, an important point for the reconstruction of jet energies.
- as gas forms the active medium, the amount of material in front of the ECAL is minimised. This reduces multiple scattering and also reduces the occupancy in the tracking chamber arising from conversions of background photons.
- it provides dE/dx information allowing particle identification.
- it allows easy identification of 'non-pointing' tracks, *i.e.* tracks which do not originate from the interaction region, thereby allowing the reconstruction of decaying neutrals, *e.g.* $\mathrm{K_S} \rightarrow \pi^+\pi^-$. This is also important in searches for signals for physics beyond the Standard Model. For example, one possible signal for Gauge Mediated SUSY Breaking (GMSB) would be the observation of kinked tracks in the process $\mathrm{e}^+\mathrm{e}^- \rightarrow \tilde{\mu}^+\tilde{\mu}^- \rightarrow \mu^+\mu^-\tilde{\mathrm{G}}\tilde{\mathrm{G}}$.

TPC Conceptual Design

The baseline design of the TPC is shown in Fig. 9. The active volume consists of two drift regions (forward/backward) each of 2.5 m in length. The inner radius, determined by the size of the forward mask system which extends inside the TPC bore, is 0.32 m and the outer radius is 1.7 m. The outer radius of the TPC plays an important rôle in determining the cost and performance of the detector. On the one hand the TPC has to be sufficiently large to achieve the desired momentum resolution for the baseline

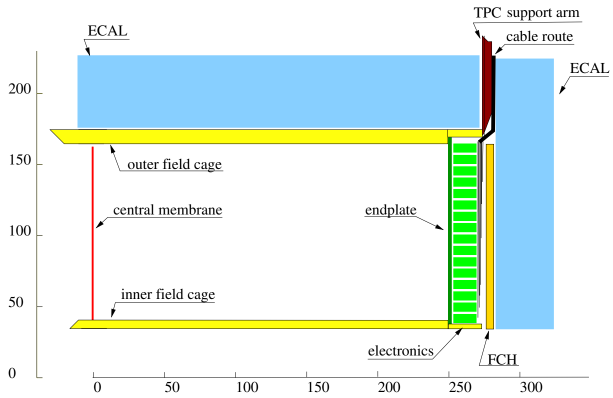

Figure 9: General layout of the TDR baseline TPC design [1] (dimensions in cm).

4 T magnetic field, on the other, the TPC dimensions determine the size of the ECAL, HCAL and solenoid, and thus significantly impacts the cost of the whole detector.

The TPC would be read out on the two end planes, each consisting of approximately 200 rings of readout pads. In the baseline design the readout pads have transverse and radial dimensions of $2 \times 6\,\mathrm{mm}^2$. The performance of the TPC depends on the choice of gas, which not only affects the resolution through the transverse and longitudinal diffusion of the drifting charge cloud but also influences the design of the field cage (as the total voltage at the cathode depends on the desired drift velocity). In addition, gas mixtures with high hydrocarbon content present a large cross-section to neutron background, leading to higher TPC occupancy. The baseline choice for the TESLA TPC is a three-gas mixture of Ar-CO_2-CH_4 (93-2-5), although there are many other options [18]. With this choice of gas a single hit resolution of $140\,\mu$m can be achieved [19]. The ultimate aim is $\sigma \sim 100\,\mu$m which can be reached using 90-10 Ar-CH_4 which has a smaller transverse diffusion constant, although it is more sensitive to neutron background. The longitudinal granularity of a TPC is limited by the longitudinal diffusion of the charge cloud. In Ar-CO_2-CH_4 the longitudinal (transverse) diffusion constants in a 4 T solenoidal field are $300(70)\,\mu\mathrm{m\,cm}^{-1/2}$. Hence, for typical drift distances of 1 m, the longitudinal spread of the electron cloud is about 3 mm. For a drift velocity of $5\,\mathrm{cm}\,\mu\mathrm{s}^{-1}$, this corresponds to a time resolution of 60 ns requiring a readout rate of at least 20 MHz.

There are two main drawbacks inherent to a TPC. Firstly, there is a significant amount of material in the endcap regions due to the endplanes and the readout electronics. Ideally the amount of material in front of the ECAL should be minimised and the goal is for the contribution from the TPC to be less than $0.3\,X_0$. Secondly, due to the finite drift time, the TPC integrates over multiple bunch crossings within a bunch train. This enhances the detector occupancy from beam background and gamma-gamma interactions [20] which could lead to a degradation in the pattern recognition capability. For a drift velocity of $5\,\mathrm{cm}\,\mu\mathrm{s}^{-1}$, the maximum drift time is approximately $50\,\mu$s. This corresponds to 160 bunch-crossings for which the estimated background is 80000 hits in the TPC at $\sqrt{s} \sim 500\,\mathrm{GeV}$ (and twice as much at $\sqrt{s} \sim 800\,\mathrm{GeV}$). However, the sensitive TPC volume corresponds to approximately 10^9 three-dimensional electronic readout pixels ($\sim 1.5 \times 10^6$ pads $\times\, 10^3$ longitudinal time samples). Consequently, the resulting occupancy from beam and gamma-gamma backgrounds is less than 1 % [20]. This would not present a significant problem for pattern recognition/track reconstruction even if the machine background calculations are wrong by a large factor.

TPC Readout

In a conventional TPC the number of drift electrons is amplified by avalanche multiplication in the high electric fields generated near the thin wires of multi-wire proportional chambers and the signal is read out via the induced charge on pads placed behind the wires. There are a number of problems with this traditional approach if applied to a TPC operating at TESLA:

- The resolution is limited by $\vec{E} \times \vec{B}$ effects in the strong magnetic field of the TESLA detector. This occurs because close to the proportional chamber wires the electric and magnetic fields are no longer parallel and electrons drifting in this region are subject to significant transverse forces which broaden the electron cloud and therefore degrade the resolution. This is significant for traditional multi-wire readout because the region over which $\vec{E} \times \vec{B}$ effects are important is determined by the relatively large separation of the wires (which sets the scale for the distance over which electrons drift with a non-zero velocity component perpendicular to the magnetic field).

- Positive ions produced in the gas amplification process migrate back into the drift region and can distort the electric field, termed ion feedback. In previous TPCs ion feedback was reduced by installing a gating plane just in front of the amplification region which effectively blocked positive ions drifting back into the TPC drift region except for after a trigger. Due to the bunch structure at TESLA and triggerless readout, this is only an option between bunch-trains.

- The large number of wires in the endplane and the structure required to keep the wires under tension constitutes a significant amount of material.

Because of the above disadvantages of conventional multi-wire readout alternative technologies form the basis of the baseline TESLA detector TPC design. Two options are currently being considered: Gas Electron Multipliers [21] (GEMs) or MicroMEGAS [22]. Here only GEMs will be discussed as MicroMEGAS share many of the advantages and difficulties of GEMs.

A GEM, shown schematically in Fig. 10, consists of two metal foils separated by a thin polymer film with a typical thickness of $50\,\mu$m. The device has a high density of small holes typically separated by $100 - 200\,\mu$m. By applying a potential difference across the two sides of the GEM, high electric fields are generated in the region of the small holes ($40 - 80\,\mathrm{kV\,cm^{-1}}$). Nearly all the electrons drifting from the TPC volume are funnelled into these holes where gas amplification occurs. The amplified charge is directly collected on readout pads located a few millimetres behind the GEM.

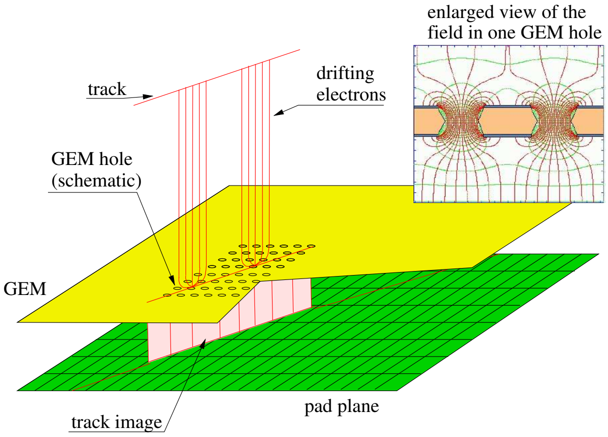

Figure 10: Schematic view of a single layer Gas Electron Multiplier (GEM).

GEMs offer a number of advantages over multi-wire readout:

- because of the small hole separation the region over which the electrons move transverse to the magnetic field is small and $\vec{E} \times \vec{B}$ effects are greatly reduced. Consequently the intrinsic resolution of the TPC is improved.

- ion feedback is naturally suppressed as the majority of the positive ions are swept onto the metal foils of the GEM and do not reach the TPC drift region (as can been seen from the electric field lines shown in Fig. 10). Ion suppression to the level 10^{-2} has already been achieved. However for stable operation of the chamber the goal is 10^{-4}. If this cannot be reached one solution would be to add a gating plane which is open for the entire TESLA bunch train.

- as there are no wires to keep under tension it should be possible to produce thinner endplanes.

GEMs have a number of advantages over wire chamber readout, however they also bring a number of new challenges. The avalanche region is relatively small and only limited amplification is achieved (typically less than a factor 100). Consequently, it is likely that a cascade of at least two GEMs will be required to achieve the necessary gas amplification, for example see [23]. In multi-wire chamber readout, the electron avalanche induces charge on the readout pads, resulting in a signal which is spread across several pads. By using a centre-of-gravity algorithm the resolution is not limited by the pad size. In GEMs and MicroMEGAS the amplified charge is directly transferred onto the readout pads. Here the electron clouds arriving at the readout planes have typical dimensions of $20 - 50\,\mu$m, determined by diffusion over the $1 - 5\,$mm drift distance from the GEM to the readout plane (for GEM towers there is further diffusion in the gaps between the GEMs). Unless the readout pad sizes are matched to the electron cloud size, which would result in a prohibitively large number of channels, the signal will be often localised to a single pad. In this case it is the pad size (nominally two millimetres) rather than the GEM hole separation ($\sim 100\,\mu$m) which determines the resolution of the device. However, in the absence of the induction signal it is still possible to achieve good resolution. A number of approaches have been considered. For example, by using "chevron" rather than rectangular shaped readout pads, as indicated in Fig. 11, it is possible to spread the charge cloud over more than one pad and obtain the necessary improvement in resolution [19]. Another promising idea is to spread the charge across a number of pads by inserting a resistive layer in front of the pads [24]. It seems likely that a solution to this particular aspect of using GEMs to readout the TPC will be found.

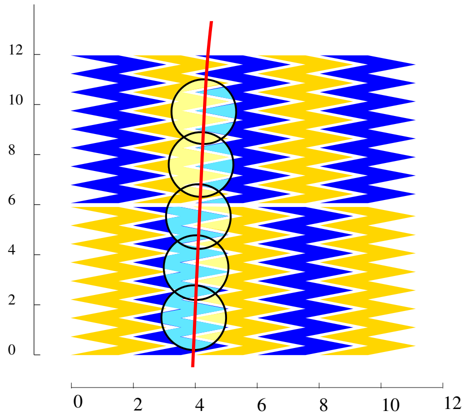

Figure 11: Possible layout of "Chevron" shaped pads, with a track superimposed to illustrate the sharing of charge between different pads (dimensions in mm) [19]. The circles indicate the typical size of the charge cloud arriving at the pads for a structure consisting of two GEMs.

TPC Summary

Since the production of the TESLA TDR there has been an active programme of R&D into the possible use of TPCs as the central tracking chamber for a detector at the TESLA linear collider. Although, to date, no major pitfalls have been identified, more work is required before it can concluded that a TPC will provide the necessary performance and stability. Fortunately there are a significant number of groups worldwide actively involved in R&D [25] work for a TPC option for a future LC detector.

Tracking Performance

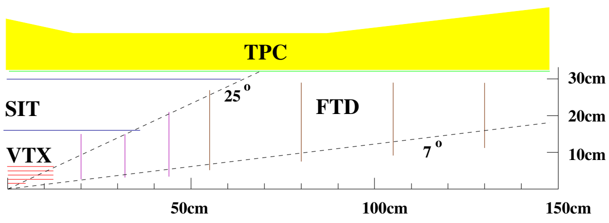

Figure 12: Layout of the TDR concept of the intermediate and forward tracking chambers [1].

In the TESLA detector design the tracking capabilities of the VTX and TPC are complemented by a series of Silicon detectors in the region between the vertex detector/beam pipe and the TPC, as shown in Fig. 12. The main purpose of these detectors is to improve the momentum resolution particularly in the forward region. The SIT consists of two cylinders of double-side Silicon strips with resolution $\sigma_{r\phi} = 10\,\mu$m. Such a detector poses few technological problems; similar detectors have already been successfully used in the DELPHI microvertex detector. The SIT is useful for the purpose of pattern recognition, providing a link between VTX and TPC tracks. However, its main purpose is to provide two well measured space points at a relatively large distance from the interaction point. Using a combination of the TPC and hits in the five layers of the VTX detector, supplemented by the SIT, the resolution goal of $\sigma_{1/p} = 5 \times 10^{-5}\,\mathrm{GeV}^{-1}$ is reached (see Table 2). It should be noted that the momentum resolution of the TESLA TDR tracking system was obtained from a full simulation of the detector [15] using sophisticated track fitting code adapted from that used at LEP [26].

Table 2: Momentum resolution for tracks in the barrel region.

Detector	$\sigma_{1/p}$
TPC	$1.5 \times 10^{-4}\,\mathrm{GeV}^{-1}$
+VTX	$0.7 \times 10^{-4}\,\mathrm{GeV}^{-1}$
+SIT	$0.5 \times 10^{-4}\,\mathrm{GeV}^{-1}$

Monte Carlo studies have been performed to determine the physics sensitivity for the above momentum resolution. These studies used a fast simulation program[27] which uses a parametrisation of the detector resolutions obtained from the full simulation. Fig 13a) shows the resulting invariant mass distribution of the $\mu^+\mu^-$ system in simulated $\mathrm{e^+e^-} \to \mathrm{HZ}$ events. The width is dominated by the natural width of the Z and not the experimental momentum resolution. Fig. 13b) shows the invariant mass of the Higgs boson as measured from the $\mu^+\mu^-$ recoil mass. Here the distribution, which has a peak at the assumed Higgs mass ($M_\mathrm{H} = 120\,\mathrm{GeV}$), displays a significant tail towards higher masses. The origins of this tail are Beamstrahlung (discussed below) and ISR.

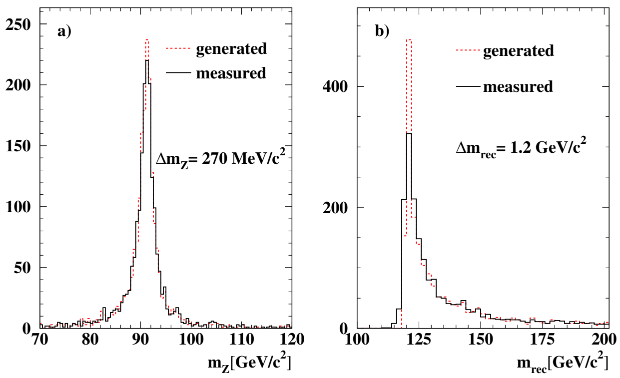

Figure 13: a) Generated and reconstructed Z mass and b) recoil mass for $\mathrm{e^+e^-} \to \ell^+\ell^-\mathrm{H}$ Higgs-strahlung events at $\sqrt{s} = 350\,\mathrm{GeV}$ (M_H=120 GeV) [1].

FORWARD TRACKING

Forward tracking is particularly important at TESLA for three main reasons:

- One undesirable aspect of a future LC is Beamstrahlung. Beamstrahlung is the induced photon radiation from an electron (positron) in one bunch in the coherent field of the positrons (electrons) in the colliding bunch. The amount of Beamstrahlung depends strongly on the machine design and corresponds to an average energy loss of around $1.5\,\%$ for TESLA [28]. The effect of Beamstrahlung on the effective centre-of-mass energy spectrum after photon radiation, $\sqrt{s'}$, is shown in Fig. 14. To make precise mass measurements, *e.g.* M_W from a threshold cross-section scan and to a lesser extent M_H from the recoil mass spectrum, the effects of Beamstrahlung must be quantified. Fortunately, the luminosity spectrum can be obtained from data by studying the acollinearity distribution of Bhabha scattering events for which the cross-section is highly forward peaked. Consequently, a LC detector requires excellent *polar angle* resolution for forward tracks [29].

- Many of the physics processes at a LC are forward-peaked, for example $\mathrm{e^+e^-} \to \mathrm{W^+W^-}$. Here, due to the highly boosted W bosons, the jets from a hadronic W-decay are not only forward-peaked but also tend to overlap.

- Missing energy is the main signature for many SUSY processes and good forward tracking is required to improve the missing-energy resolution.

For tracks with polar angles below 25° the polar angle resolution, and to lesser extent the momentum resolution, is

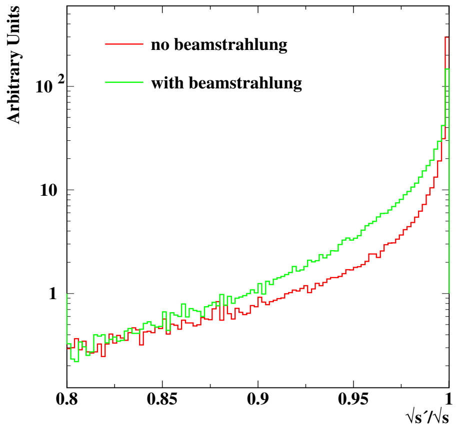

Figure 14: The $\sqrt{s'}/\sqrt{s}$ distribution for $\mathrm{e^+e^-}$ collisions at a nominal centre-of-mass energy of 500 GeV. The effects of ISR alone and ISR plus Beamstrahlung are shown [29].

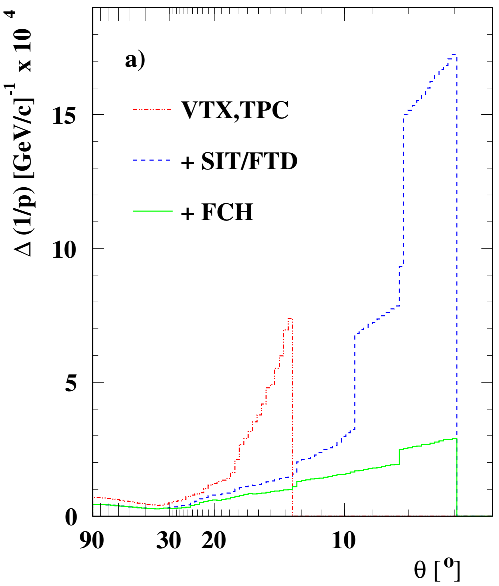

Figure 15: Momentum resolution for 250 GeV muons as a function of polar angle. In this case the FCH is the TDR straw chamber option.

improved using the forward tracking detector (FTD) which consists of a series of seven Silicon disks. The first three layers of the FTD consist of Silicon pixel detectors with a pixel size of $50 \times 300\,\mu\mathrm{m}^2$. The four layers furthest from the interaction point consist of Silicon strips with a resolution of $90\,\mu\mathrm{m}$. The excellent polar angle resolution obtained from the FTD not only allows the mean energy loss due to Beamstrahlung to be measured with a statistical precision of 5×10^{-5}, but also provides a measurement of the beam energy spread with statistical precision of 0.5×10^{-5} [29].

Forward Chambers

The FTDs primarily measure the polar angle of forward tracks. However, in the forward direction the momentum resolution of the TPC is degraded due to the decreased lever-arm and the reduced number of hits. To improve the momentum resolution in this region, forward chambers (FCH) with a point resolution of approximately $50\,\mu\mathrm{m}$, are positioned directly behind the TPC end planes. In the TESLA TDR three planes of straw tubes were foreseen. Recently it has been suggested that Silicon strip detectors forming a "Silicon Envelope" around the entire TPC would be a better choice [30] (see below). Independent of the technological choice, the importance of additional tracking in the forward region can be seen from Fig. 15 which shows the momentum resolution for 250 GeV muons as a function of polar angle when information from different detectors is included.

Silicon Envelope

It has been suggested that the TDR tracking system could be complemented by an envelope of Silicon surrounding the TPC [30]. The original proposal [31] considered only the barrel region, the Silicon External Tracker (SET). The SET would consist of three cylindrical layers of Silicon detectors just beyond the TPC at radii 160.5 cm, 165 cm and 169.5 cm. Recently this idea was extended to replacing the straw-tube FCH with a six layer Silicon tracker (Si-FCH) [30]. Preliminary studies [30] which assumed a single-layer point-resolution of $25\,\mu\mathrm{m}$ and that each layer represented 0.5 % of a radiation length, indicate that the SET could improve the momentum resolution in the barrel region by upto 20 %. However, at this stage the merits of the SET should be taken with some caution as the improvement in momentum resolution depends strongly on the assumed performance of the TPC. Nevertheless, a Si-envelope may offer other advantages:

- The addition of a precisely measured space point, outside the material of the TPC support structure could aid the calorimeter reconstruction and improve the energy flow measurement.
- The addition of the Silicon-envelope would complement the tracking in the VTX, SIT and FTD Silicon detectors, forming a large lever arm tracker independent of the TPC. As such, the Silicon-envelope would help in monitoring/calibrating the TPC.

CALORIMETRY

The majority of the interesting physics processes at a future linear collider are characterised by multi-jet final states, often accompanied by charged leptons and/or missing transverse energy associated with neutrinos or the lightest super-symmetric particles (LSPs). The reconstruction of the invariant mass of two or more jets will provide a powerful tool both for event reconstruction and for event identification. For example:

- the identification of the rare, but nevertheless important, ZHH $\rightarrow 6j$ final state from background processes will rely on the ability to identify pairs of jets with the invariant masses of the Z and Higgs;

- the identification and separation of $\nu_e\overline{\nu}_e\mathrm{W}^+\mathrm{W}^-$ and $\nu_e\overline{\nu}_e\mathrm{ZZ}$ events, of great interest in strong EWSB models, will rely almost entirely on di-jet mass reconstruction.

In general it will important to be able to identify jet pairs arising from the hadronic decays of W and Z bosons. Since the reconstruction of the invariant mass of two or more jets will play a major rôle in the analyses of numerous processes at the LC, a good measurement of jet energy is of great importance.

The LEP Experience

At LEP is was found that the jet energy resolution was limited by the ability to separate and correctly associate tracks and energy deposits in electromagnetic and hadronic calorimeters, rather than the intrinsic momentum and energy resolution of the tracking chambers and calorimeters respectively. Measurements of jet fragmentation at LEP have provided detailed information on the particle composition of jets (e.g. [32, 33]). On average, after the decay of short-lived particles, roughly 62% of the energy of jets is carried by charged particles (mainly hadrons), around 27% by photons, about 10% by long-lived neutral hadrons (*e.g.* n/K^0_L), and around 1.5% by neutrinos. The momenta of charged particles are measured accurately in the tracking detectors and the energy obtained by assuming the $\pi^\pm$ mass. Photon energies are measured in the electromagnetic calorimeter (ECAL), and the energies of neutral hadrons in the hadron calorimeter (HCAL). To obtain the energy of the jet, the information from tracks, ECAL clusters and HCAL clusters has to be combined taking into account correlated energy deposits. For example, a charged hadron will typically deposit energy in both calorimeters, while a neutral hadron may start showering in the ECAL. The most successful algorithms for jet reconstruction at LEP used the so-called *energy flow* approach, in which geometrical associations between tracks and calorimeter clusters and between clusters in the ECAL and HCAL are used to minimise the double counting of energy. Using the energy flow technique the ALEPH experiment obtained a jet-energy resolution of $\sigma_E/E = 60\%(1+|\cos\theta|)/\sqrt{E(\mathrm{GeV})}$ [34]. Although the OPAL lead-glass calorimeter had a better intrinsic energy resolution, OPAL achieved a jet-energy resolution of only $\sigma_E/E \sim 80\%/\sqrt{E(\mathrm{GeV})}$. The main reason for the relatively good performance of the ALEPH calorimeter was that it had significantly better spatial resolution, permitting better matching and separation of the various energy deposits within a jet. At LEP the beam-energy constraint used in the kinematic fits reduced the sensitivity to the jet energy resolution; despite having very different jet energy resolutions, the four LEP experiments achieved similar M_W sensitivity (a measurement where most of the information comes from the reconstructed jet-jet invariant mass distribution).

Jet-Energy Resolution

At a LC kinematic fitting will play a less significant rôle than at LEP as many final states involve missing energy and the beam energy constraint is less useful due to Beamstrahlung. Consequently, good jet-energy resolution is of paramount importance. A jet energy resolution of $\Delta E = \alpha\sqrt{E}$ leads to a di-jet mass resolution of roughly $\Delta M/M = \alpha/\sqrt{E_{jj}}$ where E_{jj} is the energy of the di-jet system. A reasonable goal is to match ΔM for the W or Z bosons to their natural widths, i.e. $\sim$ 2 GeV. Since E_{jj} $\sim$250 GeV at the LC, this suggests a goal of

$$\sigma_E/E = 30\,\%/\sqrt{E(\mathrm{GeV})},$$

which is a factor of two better than the best achieved at LEP. The importance of achieving this goal is well illustrated by considering the process $\mathrm{e}^+\mathrm{e}^- \rightarrow \nu_e\overline{\nu}_e\mathrm{W}^+\mathrm{W}^-$. If the Higgs mechanism is not responsible for Electroweak symmetry breaking then the quartic gauge coupling process, shown in Fig. 16, is of great interest; without the SM s-channel Higgs exchange contribution, the cross-section for longitudinal W-boson scattering, $\mathrm{W}^+_\mathrm{L}\mathrm{W}^-_\mathrm{L} \rightarrow \mathrm{W}^+_\mathrm{L}\mathrm{W}^-_\mathrm{L}$, grows with $\sqrt{s}$ and ultimately violates quantum mechanical unitarity. In strong EWSB scenarios it will be important fully to investigate quartic gauge couplings in both $\mathrm{e}^+\mathrm{e}^- \rightarrow \nu_e\overline{\nu}_e\mathrm{W}^+\mathrm{W}^-$ and $\mathrm{e}^+\mathrm{e}^- \rightarrow \nu_e\overline{\nu}_e\mathrm{ZZ}$. For fully-hadronic decays, the $\nu_e\overline{\nu}_e\mathrm{W}^+\mathrm{W}^-$ and $\nu_e\overline{\nu}_e\mathrm{ZZ}$ final states can only be distinguished on the basis of the invariant masses of the pairs of jets. Fig. 17 shows the improvement in separation obtained in going from a LEP-like resolution to the TESLA goal. In statistical terms the improved separation is equivalent to a 40 % increase in luminosity [35].

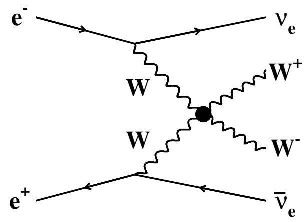

Figure 16: The process $\mathrm{e}^+\mathrm{e}^- \rightarrow \nu_e\overline{\nu}_e\mathrm{W}^+\mathrm{W}^-$.

Calorimetry at the Linear Collider

The requirements for calorimetry at a future LC can be summarised as:

- Excellent energy resolution for jets: $\sigma_E/E = 30\,\%/\sqrt{E(\mathrm{GeV})}$.

- Good energy and angular resolution for photons needed, for example, for the identification of H$\rightarrow \gamma\gamma$ events.

Table 3: Contributions from the different particle components to the jet-energy resolution (all energies in GeV). The table lists the approximate fractions of charged particles, photons and neutral hadrons in a jet and the assumed single particle energy resolution. The contribution to the overall jet energy resolution from all particles in each category is also shown. For photons and neutral hadrons this is given by the quadrature sum of the resolutions for individual particles which yields a term proportional to the total energy in that component. For charged particles only a maximum value can be given; this corresponds to there being a single charged particle in the jet. In general there will be many charged particles and this term will be negligible.

Component	**Detector**	**Energy Fraction**	**Energy Res.**	**Jet Energy Res.**
Charged Particles ($X^{\pm}$)	Tracker	$\sim 0.6\,E_{\rm jet}$	$10^{-4}\,E^2_{X^{\pm}}$	$< 3.6 \times 10^{-5}\,E^2_{\rm jet}$
Photons (γ)	ECAL	$\sim 0.3\,E_{\rm jet}$	$0.11\,\sqrt{E_\gamma}$	$0.06\,\sqrt{E_{\rm jet}}$
Neutral Hadrons (h^0)	HCAL	$\sim 0.1\,E_{\rm jet}$	$0.40\,\sqrt{E_{h^0}}$	$0.13\,\sqrt{E_{\rm jet}}$

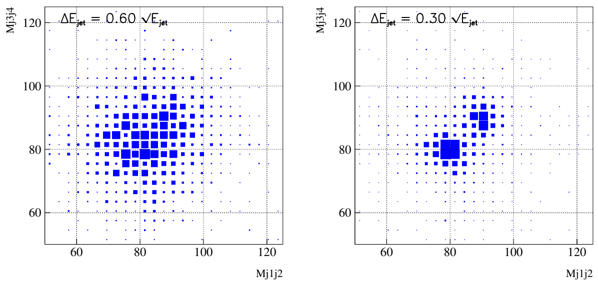

Figure 17: Impact of the jet energy resolution on the separation of $\nu_e\overline{\nu}_e{\rm W^+W^-}$ and $\nu_e\overline{\nu}_e{\rm ZZ}$ final states where both gauge bosons decay hadronically [35]. The first plot shows the separation for the best LEP jet-energy resolution, $\sigma_E/E = 60\,\%/\sqrt{E({\rm GeV})}$, and the second shows the separation for the TESLA goal of $\sigma_E/E = 30\,\%/\sqrt{E({\rm GeV})}$.

- The ability to identify non-pointing photons which can arise, for example, in GMSB scenarios where a long-lived neutralino may decay in the detector volume to a photon and an unobserved stable gravitino, $\tilde{\chi}^0_1 \to \gamma\tilde{\rm G}$.
- Excellent hermeticity.
- Ideally both the ECAL and HCAL should be placed inside the magnet coil to avoid degradation in energy resolution. For this to be affordable the calorimeters have to be compact.

Of the above requirements it is that of jet-energy resolution which drives the calorimeter design. To understand the dominant source of uncertainty it is useful to decompose the jet-energy resolution into its components. In an ideal world one would measure the energy of charged particles using the tracking chambers, the energy of photons using the ECAL and the energy of neutral hadrons using the HCAL. Table 3 (adapted from [36]) shows the different contributions to the jet-energy resolution assuming no double-counting of energy deposits. It should be noted that although the neutral hadron component comprises only $10\,\%$ of the jet energy this is the largest single contribution to the uncertainty. From the sum of the contributions from the individual components, a jet-energy resolution of $\sigma_E/E = 14\,\%/\sqrt{E({\rm GeV})}$ is obtained. This is far better than the best achieved for the TESLA TDR detector, $\sigma_E/E = 30\,\%/\sqrt{E({\rm GeV})}$. From this it is clear that, in practice, the dominant contribution to the jet-energy uncertainty comes from double-counting energy deposits in more than one detector component or missing energy deposits due to overlapping tracks and showers. Consequently, one can conclude that the jet-energy resolution is driven mainly by the ability to resolve energy deposits from different particles. This is particularly difficult in the dense environment of (potentially highly boosted) hadronic jets at a LC, as can be seen from Fig. 18. Consequently, for the purposes of jet-energy resolution granularity is more important than energy resolution.

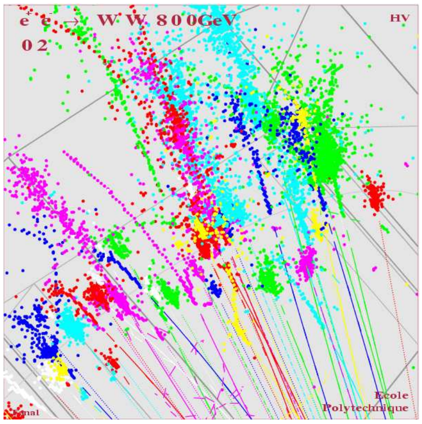

Figure 18: View of a di-jet in ${\rm e^+e^-} \to {\rm W^+W^-}$ at $\sqrt{s} =$ 800 GeV [35].

TESLA Calorimeter Concept

The calorimeters at TESLA should be able to:

- *separate of energy deposits from different nearby particles.* Therefore the ECAL should have a small Molière radius, $\rho_{\rm M}$, to limit the transverse spread of electromagnetic showers and a high lateral segmentation (of the order ρ_M).

- *discriminate between electromagnetic and hadronic showers.* Therefore the ECAL (and HCAL) should have a large ratio of the interaction length, λ_I, to the radiation length, X_0, so that hadronic showers start relatively deep in the calorimeter. It also implies longitudinal as well as transverse segmentation of the calorimeters.

- *contain electromagnetic showers in the ECAL.* This suggests that the ECAL should be $\sim 20 - 25\,X_0$ in depth, sufficient to contain the highest energy showers. This is a further argument for choosing a material with small X_0 in order to arrive at a compact ECAL.

The preferred solution adopted for the TESLA TDR, shown in Fig. 19 envisages a Silicon-tungsten ECAL, followed by an HCAL, both located inside the magnet coil. The barrel regions have an octagonal geometry. Specialised calorimetry in the forward region would complete the angular coverage.

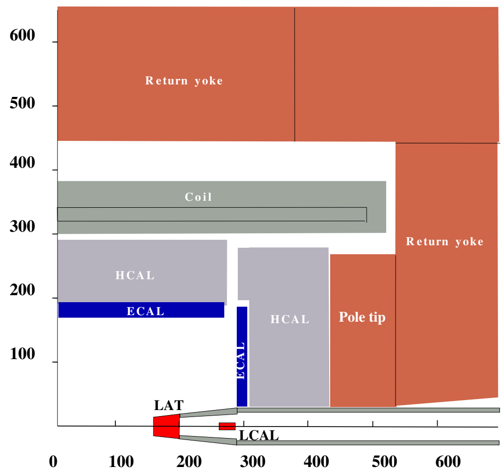

Figure 19: Side view of the TESLA TDR calorimeters [1] (dimensions in cm).

Electromagnetic Calorimeter

Tungsten is an attractive choice for the showering medium in the ECAL, having a very low radiation length, a small Molière radius of 9 mm and a large ratio of λ_I/X_0, see Table 4. By using Silicon as the detecting medium, the gaps between tungsten layers can be kept thin, so that the whole ECAL of 24 radiation lengths thickness can be fitted into a thickness of about 20 cm. Keeping the gaps between the tungsten layers to a minimum also avoids a significant increase in the effective Molière radius of the Si-W sandwich. The transverse granularity of the Silicon readout, *i.e.* the size of the Silicon pads is determined by the Molière radius, which defines the transverse size of electromagnetic showers. If the pad size is significantly greater than the Molière radius the shower can only be localised to within the area of one pad and the spatial resolution is

Table 4: Comparison of interaction length, λ_I, radiation length, X_0, and Molière radius, $\rho_{\rm M}$, for Iron, Copper, Tungsten and Lead. Also given is the ratio of λ_I/X_0.

material	$\boldsymbol{\lambda_I}$**/cm**	$\boldsymbol{X_0}$**/cm**	$\boldsymbol{\rho_{\rm M}}$**/cm**	$\boldsymbol{\lambda_I/X_0}$
Fe	16.8	1.76	1.69	9.5
Cu	15.1	1.43	1.52	10.6
W	9.6	0.35	0.93	27.4
Pb	17.1	0.56	1.00	30.5

degraded. Consequently a pad size of $\sim$1 cm^2 is envisaged. The present design of the ECAL has 40 longitudinal samples. The high granularity leads to an excellent angular resolution for photons:

$$\sigma_\theta = (0.063/\sqrt{E/\mathrm{GeV}} \oplus 0.024)\,\mathrm{mrad},$$

allowing the identification of 'non-pointing' photons arising from possible GMSB signals from purely neutral decays in the TPC volume. The jet-energy resolution of the TDR ECAL design yields an energy resolution for single photons of

$$\sigma_{E_\gamma}/E_\gamma = (0.11/\sqrt{E_\gamma/\mathrm{GeV}} \oplus 0.01).$$

Hadronic Calorimeter

The total ECAL depth for normal incident particles corresponds to $24\,X_0$ (sufficient to mostly contain even the highest energy electromagnetic showers) but corresponds to only $0.9\,\lambda_I$, consequently hadronic showers tend to develop late in the ECAL. For the purposes of energy-flow the HCAL should be highly segmented, both in the transverse and longitudinal directions. However, the overall cost impact of the HCAL design is determined by its size, which determines the coil radius. Hence cost arguments suggest a compact detector and the ideal showering material would be Tungsten which has a particularly short hadronic interaction length (see Table 4). Unfortunately Tungsten is relatively expensive and price considerations tend to favour using stainless steel which has a somewhat larger λ_I. The total area of the active layers of the HCAL is approximately $5000\,\mathrm{m}^2$, which would require 5×10^7 electronics channels for a $1\,\mathrm{cm}^2$ lateral segmentation. To avoid the prohibitively high cost of the readout a compromise is likely to be made: either degrading the lateral segmentation, which reduces the number of channels, or by reducing the information read out from a single channel. In the latter case, the *digital HCAL* option, multiple active elements are read out on a single channel. For the digital readout one records whether or not there was an energy deposit in a particular detector cell but not amount of energy itself, *i.e.* a simple binary yes/no outcome. The baseline design consists of a 1 m thickness HCAL consisting of approximately 40 layers, providing $4.5\lambda_I$ ($6.2\lambda_I$) of material in the barrel (endcap) region. To reduce the number of readout channels the layers are grouped into 9 (12) longitudinal readout layers in the barrel (endcap).

Among the preferred options for the HCAL are stainless steel plates instrumented with either $\sim 5 \times 5\,\mathrm{cm}^2$ scintillator tiles (providing analogue readout) or resistive plate chambers (RPCs) providing digital readout with a granularity of between $1 \times 1\,\mathrm{cm}^2$ and $2 \times 2\,\mathrm{cm}^2$. The digital option has the advantage that multiple detector elements can be readout on the same electronics channel, thus reducing the cost of the associated readout which would otherwise be prohibitively high for a highly segmented large volume HCAL. The choice between a moderately segmented HCAL with analogue readout or a highly segmented HCAL with digital readout is a matter of great debate and ongoing studies (*e.g.* see [37]). Naively one might expect the digital option to result in a degraded energy resolution as energy is not explicitly recorded. However, for hadronic showers this is not necessarily the case. Hadronic showers consist of a number of distinct components: the ionisation from the primary particle (if charged); a relatively compact electromagnetic component *e.g.* arising from π^0 decays; and a broad (typically transverse size of a few λ_I) hadronic component from secondary hadrons. The response of the HCAL to these different components influences the performance:

- The charged hadron (predominantly $\pi^{\pm}$) component of the shower is essentially track-like, consisting of a number of near minimum ionising particles. Here the total path length, summed over all tracks, provides a good energy estimate. This is exactly what is measured in the digital option, providing that the typical transverse separation of the particles is larger than the segmentation of the HCAL. The energy resolution for the charged hadron component in the analogue option has an additional contribution. In an analogue sampling calorimeter it is the ionisation in the active detector volume that is recorded rather than the total energy. For a charged particle crossing a single active detector element the ionisation follows the (asymmetric) Landau distribution which has a long tail towards high values. Consequently a single sample of the ionisation energy loss of a single charged hadron is subject to large fluctuations. As only a small fraction of the total energy loss is sampled, the inclusion of these large fluctuations may degrade the energy resolution for the track-like component of the shower.

- The electromagnetic component of a hadronic shower consists of many electrons, positrons and photons in a small transverse region, information which is lost in the digital option. Hence the electromagnetic component can only be directly measured in the analogue HCAL, although in the digital HCAL there is information in shower size.

- The TESLA HCAL designs are implicitly non-compensating, having different responses for the hadronic and electromagnetic components of the shower. In a highly segmented calorimeter it might be possible to identify tracks and electromagnetic showers, allowing the possibility of software compensation. This argues for a transverse granularity of order the Molière radius. In addition the higher granularity of the digital HCAL would provide better separation of energy deposits from nearby hadronic showers, potentially improving the performance of the energy flow algorithm.

Based on the above arguments it is difficult to foresee which option will give the best jet-energy performance in the context of an energy-flow algorithm. Since many of the effects are subtle, sophisticated Monte Carlo simulation and energy flow algorithms will be required to address this interesting question of digital versus analogue HCAL.

Calorimeter Performance

As an example of the TDR calorimeter performance, Fig. 20 shows the distribution of reconstructed minus true Z mass for jets from $\mathrm{e^+e^-} \to \mathrm{q\overline{q}}$ at $\sqrt{s} = M_\mathrm{Z}$ obtained using for the digital HCAL option [35]. A mass resolution of 2.89 GeV is achieved, which corresponds to a jet energy resolution of $0.3/\sqrt{\mathrm{E(GeV)}}$, the TESLA goal.

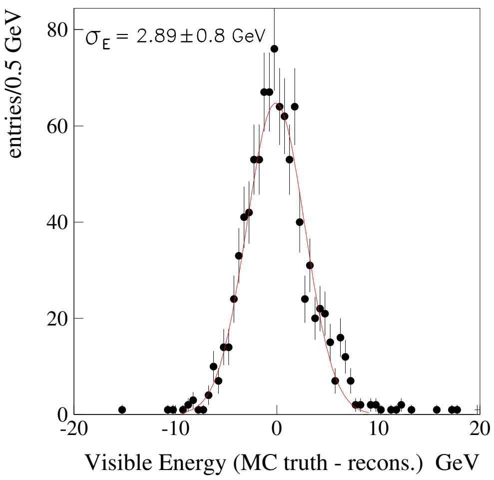

Figure 20: The jet-jet mass resolution for Z decays at rest [35].

Finally, given the relatively large cost of the TDR calorimeters, it is worth re-emphasising the physics impact. A good example of the importance of excellent jet-energy resolution is the SM process $\mathrm{e^+e^-} \to \mathrm{ZHH} \to \mathrm{q\overline{q}b\overline{b}b\overline{b}}$. This process involves the trilinear Higgs coupling, as shown in Fig. 21, providing a direct probe of the Higgs potential. Here the signal cross-section is small (~ 0.5 fb) and the background large. In addition, the six jet final state results in a large combinatorial background arising from the association of the six jets to the two Higgs bosons and the Z. However, providing one has sufficiently good jet-energy resolution, the invariant masses of the re-

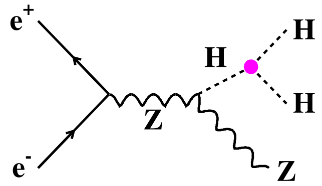

Figure 21: The process $e^+e^- \to$ ZHH which probes the Higgs trilinear self-coupling.

constructed di-jet pairs may be used to significantly reduce the backgrounds. A useful discriminating variable is

$$D = \sqrt{(m_{12} - m_H)^2 + (m_{34} - m_H)^2 + (m_{56} - m_Z)^2},$$

where the m_{ij} are the reconstructed invariant masses of the jet pairs hypothesised as being associated with Higgs/Z boson. Figure 22 shows the distributions of D for signal and background for two cases: $\sigma_E/E = 0.3/\sqrt{E(\mathrm{GeV})}$ (the TESLA goal) and $\sigma_E/E = 0.6(1 + |\cos\theta|)/\sqrt{E(\mathrm{GeV})}$ (LEP-like) [38]. The increased significance of the signal above the background expectation in going from a LEP-like jet-energy resolution to the TESLA goal is equivalent to a fourfold increase in luminosity. Given the smallness of the cross-section, a jet-energy resolution of a least $\sigma_E/E = 0.35/\sqrt{E(\mathrm{GeV})}$ is required to establish a signal for an integrated luminosity of 1 ab^{-1}. Here the excellent jet-energy resolution makes the difference between observing the process or not.

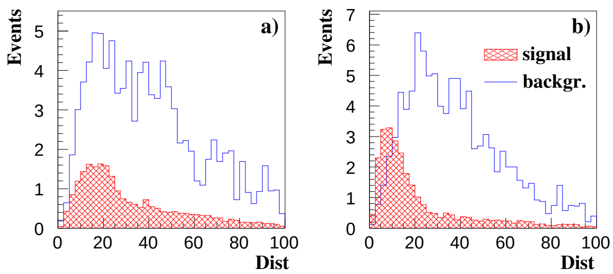

Figure 22: Distributions of the discriminating variable D for ZHH $\to$ 6 jet signal and background, for two values of jet energy resolution: a) $\sigma_E/E = 0.6(1 + |\cos\theta|)/\sqrt{E(\mathrm{GeV})}$ (LEP-like); b) the TESLA goal of $\sigma_E/E = 0.3/\sqrt{E(\mathrm{GeV})}$.

OTHER DETECTORS

In addition to the detector components described above, the TESLA TDR detector includes muon chambers and forward calorimeters, described briefly below.

Muon Chambers

The basic task of the muon system is to identify muons which penetrate the HCAL. The muon system would be embedded in the 2 m thickness of iron of the magnetic return yoke, see Fig. 2. The muon system may also be useful as a “tail-catcher” for hadronic showers which are not fully contained in the HCAL. A number of options exist for the muon detectors, both Plastic Streamer Tubes and RPCs are considered in the TESLA TDR.

Forward Calorimeters

The ECAL coverage of the TESLA detector concept is completed by two devices in the very forward region: the Low Angle Tagger (LAT) and the Luminosity Calorimeter (LCAL), as indicated in Fig. 19. The LAT improves the detector hermeticity by providing calorimetric coverage down to polar angles of 30 mrad. In addition, the LAT allows a precise Measurment of the luminosity using low angle Bhabha scattering events. It is foreseen that the LAT would be a Silicon-Tungsten sampling calorimeter along the lines of the luminosity monitors employed by ALEPH[39] and OPAL[40]. The LCAL covers the region down to polar angles of 5 mrad; its main purpose is to provide fast monitoring of the luminosity and beam. The backgrounds in this low angle region are high and a Tungsten sampling calorimeter with either oxygenated Silicon or Diamond sensors[41] are being considered.

CONCLUSIONS AND OUTLOOK

Two years after the publication of the Tesla TDR[1], the basic detector concept remains the same, providing a viable route to achieving the basic performance goals necessary at a future LC. The emphasis now has shifted towards R&D to investigate the technical issues surrounding the main detector components: there are a number of active R&D programmes investigating the issues specific to the operation of a TPC at a future LC; the CALICE collaboration [42] will soon commence a major test-beam study of the proposed ECAL and HCAL designs; and there are a number groups investigating possible Silicon technologies for the VTX detector. In addition to the technical issues, there many open questions. For example, is a Silicon central tracker a realistic alternative to a TPC ? In this case one would have essentially the same (*i.e.* Silicon-based) technology for the entire detector which is an attractive idea. There is also the important question of the analogue versus digital versions of the HCAL. Furthermore, there are many issues related to the optimisation of the detector design, for example, what is the optimal length and outer radius of the TPC ? To address these issues will require full simulation studies of the whole detector as the design of one detector component may affect the performance of another. For example, the TPC outer radius impacts not only the tracking performance, but also the ECAL inner radius and the jet-energy resolution. Studies of this kind, considering the performance of the detector as whole, are just starting in earnest. It is important that we obtain answers to many of these questions as soon as possible as, in the not too distant future, hopefully we will have to start designing and constructing the real detector.

ACKNOWLEDGEMENTS

I would like to acknowledge the following people for many useful and illuminating discussions over the past year: Jean-Eudes Augustin, Jean-Claude Brient, Chris Damerell, David Miller, Vasily Morgunov, Markus Schumacher, Ron Settles, Jan Timmermans, Henri Videau, and David Ward.

REFERENCES

[1] TESLA Technical Design Report, DESY 2001-011, ECFA 2001-2009.

[2] The ALEPH, DELPHI, L3 and OPAL Collaborations, the LEP Electroweak Working Group, and the SLD Electroweak and Heavy Flavour Working Groups, "A Combination of Preliminary Electroweak Results and Constraints on the Standard Model", hep-ex/0312023.

[3] M. Thomson, "The Measurement of the Mass and Width of the W Boson at LEP", to appear in the proceedings of the EPS Conference on HEP, Aachen, July 2003.

[4] CMS Collaboration, "The Magnet Project", Technical Design Report, CERN/LHCC 97-10, May 1997.

[5] C. Damerell and K. Stefanov, "A CCD-based Vertex Detector for the Future Linear Collider", LC-DET-2003-060.

[6] M. Winter *et al.*, "Development of CMOS Sensors for a Linear Collider Vertex Detector", DESY Physics Research Committee progress report, May 2003. `http://www-zeus.desy.de/~gregork/MAPS/Papers/MAPS_PRC_REPORT_2003.pdf`.

[7] M. Battaglia, "Hybrid Pixel Detector Development for the Linear Collider Vertex Detector", Proc. IEEE Nuclear Science Symposium, Lyon, October 2000. `http://home.cern.ch/~caccia/IEEE.pdf`.

[8] P. Fischer *et al.*, "A DEPFET based pixel vertex detector for the detector at TESLA", LC-DET-2002-004.

[9] S.M. Xella-Hansen, D.J. Jackson, R. Hawkings, and C. Damerell, "Flavour Tagging Studies for the TESLA Linear Collider", LC-PHSM-2000-021.

[10] S.M. Xella-Hansen, M. Wing, D.J. Jackson, N. de Groot and C. Damerell, "Update on Flavour Tagging Studies for the Future Linear Collider using the BRAHMS simulation", LC-PHSM-2003-061.

[11] D. Jackson, Nucl. Instr. and Meth. **A388** (1997) 247.

[12] ALEPH Collaboration, D. Buskulic *et al.*, Phys. Lett. **B313** (1993) 535.

[13] OPAL Collaboration, G. Abbiendi *et al.*, Eur. Phys. J. **C8** (1999) 217.

[14] S. Giani *et al.*, "GEANT Detector Description and Simulation Tool", CERN Program Library Long Writeup W5013.

[15] T. Behnke *et al.*, "BRAHMS: A Monte Carlo for a Detector at a 500/800 GeV Linear Collider", LC-TOOL-2001-005.

[16] P.S. Marrocchesi *et al.*, Nucl. Instr. and Meth. **A283** (1989) 573.

[17] Delphi Collaboration, C. Brand *et al.*, Nucl. Instr. and Meth. **A283** (1989) 576.
Delphi Collaboration, P. Abreu *et al.*, Nucl. Instr. and Meth. **A378** (1996) 57.

[18] M. Gruwe, "Gas Studies for a TPC of a detector for the future linear collider TESLA", LC-DET-1999-003-TESLA.

[19] M. Shumacher, "Pad readout geometries for a TPC with GEM readout for the TESLA linear collider", LC-DET-2001-014.

[20] C. Hensel, "Beam Induced Background at a TESLA Detector", LC-DET-2000-001.

[21] F. Sauli, Nucl. Instr. and Meth. **A386** (1997) 531.

[22] Y. Giomataris *et al.*, Nucl. Instr. and Meth. **A376** (1996) 29.

[23] M. Killenberg, "Modelling and Measurement of Charge Transfer in Multiple GEM Structures", LC-DET-2002-022.

[24] M.S. Dixit, J. Dubeau, J.-P. Martin and K. Sachs, "Position Sensing from Charge Dispersion in Micro-Pattern Gas Detectors with a Resistive Anode", LC-DET-2003-080.

[25] The LC TPC Group, R. Settles *et al.*, "A TPC for a Future Linear Collider", LC-DET-2002-008.

[26] T. Behnke *et al.*, "Performance study of the proposed TESLA detector using a realistic track reconstruction package", LC-DET-2001-029.

[27] M. Pohl and H.J. Schreiber, "SIMDET-Version 3: A parametric Monte Carlo for a TESLA detector", DESY 99-030.

[28] See for example contributions by R. Brinkmann, T. Tauchi and K.A. Thompson *et al.*, in Vol.2 of the Proceedings of the Worldwide Study on Physics and Experiments with Future Linear e^+e^- Colliders, Stiges, April 1999.

[29] K. Moenig, "Measurement of the Differential Luminosity using Bhabha events in the Forward-Tracking region at TESLA", LC-PHSM-2000-060.

[30] J.E. Augustin *et al.*, "A Silicon Envelope for the TPC", LC-DET-2003-013.

[31] J.E. Augustin, M. Berggren and A. Savoy-Navarro, "Study of a Silicon External Tracker: SET", LC-DET-2001-075.

[32] I.G. Knowles and G.D. Lafferty, J. Phys. **G23** (1997) 731.

[33] M. G. Green, S. L. Lloyd, P. N. Ratoff and D. R. Ward, "Electron-Positron Physics at the Z", IoP Publishing (1998).

[34] ALEPH Collaboration, D. Buskulic et al., Nucl. Inst. Meth. **A360** (1995) 481.

[35] J.-C. Brient and H. Videau, "The calorimetry at the future e^+e^- linear collider", LLR 02-001, hep-ex/0202004 (revised June 2003).

[36] V. Morgunov, proceedings of the Calor2002 conference, Caltech, March 2002.

[37] S. Magill, "Comparison of simulated analog versus digital energy measurement in a finely-segmented hadron calorimeter", LC-DET-2003-009.

[38] F. Badaud et al., *Si-W calorimeter performances*, LC-DET/2001-058.

[39] D. Bederede *et al.*, ALEPH Collaboration, Nucl. Instr. and Meth. **A365** (1995) 117.

[40] G. Abbiendi *et al.*, OPAL Collaboration, Eur. Phys. J. **C14** (2000) 373.

[41] T. Behnke, M. Doucet, N. Ghodbane and A. Imhof, "Radiation hardness and linearity studies for a diamond luminosity calorimeter", LC-DET-2002-001.

[42] The CALICE Collaboration, see for example: `http://polywww.in2p3.fr/flc/calice.html`.